ARTICLE

Easy-Plane to Easy-Axis Anisotropy Switching in a Co(II) Single-Ion Magnet Triggered by Diamagnetic Lattice

Received 00th January 20xx,
Accepted 00th January 20xx

DOI: 10.1039/x0xx00000x

Joscha Nehrkorn,‡[a,b,c,d] Igor A. Valuev,‡[e,f] Mikhail A. Kiskin,[g] Artem S. Bogomyakov,[e,f] Elizaveta A. Suturina,[f,h] Alena M. Sheveleva,[e,f] Victor I. Ovcharenko,[e] Karsten Holldack,[a] Carmen Herrmann,[c] Matvey V. Fedin,[e,f] Alexander Schnegg[a,d,*] and Sergey L. Veber[e,f,*]

Single-Ion Magnets (SIMs) with large magnetic anisotropy are promising candidates for realization of single-molecule based magnetic memory and qubits. In most cases SIMs are obtained and characterized as magnetically-concentrated compounds, and creation of materials with magnetically uncoupled spatially separated ions requires dilution in a diamagnetic matrices. Initially optimized in the bulk state, the inherent magnetic properties of a SIM might worsen upon magnetic dilution. Contrary to these concerns, we report that magnetic behavior can be drastically improved by embedding SIMs in a non-isostructural diamagnetic host lattice. We have clearly demonstrated that progressive dilution of a Co^{II} complex by diamagnetic Zn^{II} ions ($[Co_xZn_{(1-x)}(piv)_2(2\text{-}NH_2\text{-}Py)_2]$, x=1÷0) leads to switching of magnetic anisotropy from easy-plane to easy-axis type. Structural analysis reveals that upon increasing the Zn:Co dilution ratio beyond a threshold of 50 % the distorted tetrahedral Zn coordination structure is superimposed on the remaining Co ions, which were initially in a distorted octahedral environment. This structural change is accompanied by an abrupt change of the magnetic relaxation times caused by switching from easy-plane to easy-axis type anisotropy. Changes of the static and dynamic magnetic properties are monitored by variable frequency electron paramagnetic resonance spectroscopy and AC susceptibility measurements. Complementary quantum chemical *ab initio* calculations quantify and predict the influence of structural changes on the electronic structure and thereby the character and the size of the magnetic anisotropy. Thus, magnetic dilution can be employed to hit two goals at once, the creation of isolated magnetic centers and the optimization of their magnetic characteristics. The present demonstration on a particular Co^{II}-SIM outlooks a straightforward general strategy, where proper selection of a diamagnetic lattice and subsequent doping of target ions yields isolated SIM units with advanced magnetic properties.

1. Introduction

Single-molecule magnets (SMMs) are subject to significant research efforts of chemists and physicists due to their prospective appealing applications in high-density information storage and molecular spintronics devices.[1-6] The key functional property of SMMs, i.e. the ability to preserve unequilibrium magnetization for a long enough time, relies on the type and magnitude of magnetic anisotropy exhibited by a particular SMM.[7-10] In this regard, single-ion magnets (SIMs) were recently evidenced as most promising systems with largest anisotropy barriers and highest magnetization blocking temperatures.[11-16] Among them, transition metal ion (TMI) complexes represent an ideal platform for knowledge-based SIM design, due to the accumulated insight in their magneto-structural correlations.[17, 18] Significant attention in this context has been devoted to Co(II), where large first order spin-orbit coupling (SOC) can lead to the very large anisotropies.[17, 19-25]

While most of the SMM research is being done on bulk materials, breakthrough SMM applications require the physical ability to address individual magnetic centers with controllable interactions between them. In certain cases spectroscopic approaches can be used to suppress magnetic interactions between neighboring SMMs.[26] However, more generally, moving one step closer to real spin devices requires spatial separation of SMMs, which can be achieved, e.g., by grafting on surfaces[27-30] or doping into host lattices of diamagnetic analogues (magnetic dilution). Apart from practical appeal, the latter is also of great fundamental interest to disentangle inter- and intramolecular SMM interactions. Therefore, magnetic dilution has become a widespread technique in SMM research. It proved to be useful for verifying the molecular origin of slow relaxation of magnetization[31] and elucidating the complex multiple relaxation processes.[32, 33] This strategy has also been successfully used for exploring the role of intermolecular dipolar interactions.[34-37] In some cases significant increase of the magnetic relaxation times upon dilution was observed.[38-42]

[a] Helmholtz-Zentrum Berlin für Materialien und Energie, Berlin, Germany
[b] Department of Chemistry, University of Washington, Seattle, WA, United States
[c] Institut für Anorganische und Angewandte Chemie, Universität Hamburg, Hamburg, Germany
[d] Max Planck Institute for Chemical Energy Conversion, Mülheim/Ruhr, Germany
[e] International Tomography Center SB RAS, Novosibirsk, Russia
[f] Novosibirsk State University, Novosibirsk, Russia
[g] N.S. Kurnakov Institute of General and Inorganic Chemistry, Moscow, Russia
[h] Department of Chemistry, University of Bath, Claverton Down, Bath, BA2 7AY, UK
‡ These authors contributed equally.
Electronic Supplementary Information (ESI) available: [details of any supplementary information available should be included here]. See DOI: 10.1039/x0xx00000x

These investigations were relying on the assumption that embedding a SMM in a diamagnetic lattice would only change its interspin interactions but not the intramolecular magnetic properties of the magnetic core unit. Indeed, this is the case if the diamagnetic lattice and the SMM are structurally completely equivalent. However, this assumption should be taken with care. For instance, diamagnetic Zn(II) ($3d^{10}$) is widely used for magnetic dilution,[37, 40, 43] but its coordination environment often deviates from that of many TMI-based SMMs. In such cases, doping the Co(II) molecules into structurally different diamagnetic Zn(II) lattice results in changing the geometry of the former due to the chemical pressure of the latter, as was shown earlier for spin-crossover compounds.[44-46] This raises the question: to what extent may structural differences between a diamagnetic host and a given SMM influence the intramolecular magnetic characteristics?

Herein, we report that native magnetic properties of SIMs can be drastically improved by their embedding in a diamagnetic host lattice of relevant structure. X-ray diffraction analysis reveals that exchange of paramagnetic Co(II) ($S = 3/2$) against diamagnetic Zn(II) in crystals composed of $[Co_xZn_{(1-x)}(piv)_2(2\text{-}NH_2\text{-}Py)_2]$ (**1**$_x$, with $x = 1$, 0.9, 0.75, 0.5, 0.25, 0.1, 0.03, 0.01, 0) alters the coordination geometry from distorted octahedral to distorted tetrahedral, beyond a Zn:Co dilution ratio of 50 %. This structural change is accompanied by an increase of the magnetization relaxation time measured at 2 K by more than five times. Structure-induced changes of the equilibrium magnetic properties are determined by electron paramagnetic resonance (EPR) experiments at X-band (9.4 GHz) and THz frequencies. Thereby, we are able to unequivocally identify a switch from easy-plane to easy-axis anisotropy. The experimentally observed correlation between dilution-induced structural changes and switching of the magnetic properties is rationalized by quantitative magneto-structural correlations obtained from SOC-NEVPT2 calculations. We suggest that this particular study leads to a formulation of a more general strategy for design of magnetically-diluted SMMs using non-isostructural diamagnetic host lattices.

2. Results and discussion

Single-crystal structures of $[Co_xZn_{(1-x)}(piv)_2(2\text{-}NH_2\text{-}Py)_2]$ (**1**$_x$) were obtained for samples **1**$_x$ with $x = 1$, 0.9, 0.75, 0.5, 0.25, 0.1 and 0. Pure Co(II) and Zn(II) crystals (**1**$_1$ and **1**$_0$, respectively) crystallize in the monoclinic space group $P2_1/c$, but with different cell parameters (see Table S2). Structures of pure compounds **1**$_1$ and **1**$_0$ are depicted in Figures 1 (b) and 1 (a), respectively. In **1**$_1$, the metal ion is in a distorted octahedral ligand environment. The corresponding shape measure[47] is $S_Q(O_h)$ = 4.12. The ligand environment for **1**$_0$ is closer to tetrahedral, with $S_Q(T_d)$ = 1.04. Fig. 1 (c) shows changes in structure and magnetic properties induced by gradual dilution. It displays the bond length from the metal to one of the coordinating oxygen atoms and the spin ground state splitting (see Figure 3 and SI) *vs.* Co(II) concentration.

All samples except **1**$_{0.5}$ crystallize in one crystalline phase according to powder X-ray diffraction (PXRD) (see Figures S2–S9). For **1**$_{0.5}$, two phases contributing with 92 % and 8 % were observed (see Figure S5). In this case, only the predominant phase is further considered. A gradual decrease of Co(II) concentration in **1**$_1$, **1**$_{0.9}$, **1**$_{0.75}$, and **1**$_{0.5}$ leads to modest variations in bond lengths. By contrast, much more pronounced changes are observed for a further decrease of Co(II) concentration from **1**$_{0.5}$ to **1**$_{0.25}$. The resulting structure is very similar to **1**$_{0.1}$ and **1**$_0$. Hence, in the further discussion we distinguish between the two groups as high-concentration materials (HCM), **1**$_1$, **1**$_{0.9}$, **1**$_{0.75}$, and **1**$_{0.5}$, and low-concentration materials (LCM), **1**$_{0.25}$, **1**$_{0.1}$, **1**$_{0.03}$, **1**$_{0.01}$ (the latter two were only studied by X-band EPR). Further structural details can be found in the ESI.

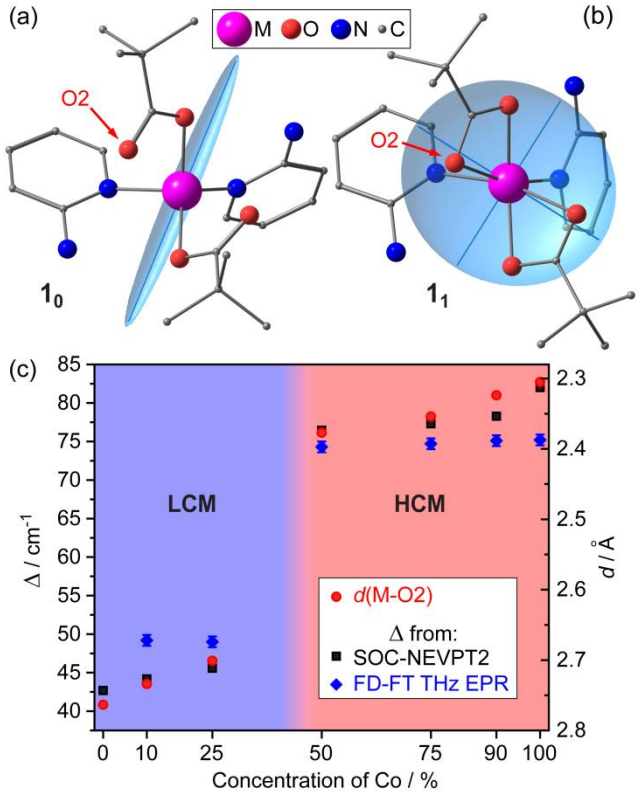

Figure 1: Host lattice induced changes of the ligand structure affect Co(II) magnetic anisotropy in Co depleted (LCM) and Co rich (HCM) materials. (a) and (b) depict molecular structures of **1**$_0$ and **1**$_1$, respectively. M refers to the metal (either Co or Zn). Tensors representing the anisotropic response of the ground state Kramers doublet to a magnetic field as calculated by SOC-NEVPT2 are shown in light blue alongside the molecular structures. In **1**$_1$ the metal ion is in a distorted octahedral coordination environment and shows easy-plane anisotropy (*i.e.* an oblate tensor). **1**$_0$ features a tetrahedral coordination environment and easy-axis anisotropy (prolate tensor). (c) Zero-field spin ground state splittings Δ extracted from THz-EPR experiments (black rectangles) and calculated by SOC-NEVPT2 (blue diamonds). A steep increase of Δ with increasing Co(II) content can be observed around 50 % of Co(II) concentration. This anisotropy change is caused by the structural modifications of the first ligation shell of Co(II) ion, which can be traced, e.g., via corresponding bond lengths. The bond length between the metal and the oxygen atom O2 is shown (red circles and *y*-scale on the right). Related plots for the remaining atoms in the first coordination shell are shown in the ESI (see Table S3 and Figures S1 & S33).

Many applications of SMMs are determined by the relaxation times of their magnetization. This property can be conveniently quantified by AC susceptibility measurements [48]. For **1**$_1$, **1**$_{0.9}$, **1**$_{0.75}$, **1**$_{0.5}$, **1**$_{0.25}$ and **1**$_{0.1}$ out-of-phase AC susceptibilities were measured under an applied DC field of 200 mT. Subsequently relaxation times τ were determined (see Figure 2 and ESI). A striking difference in the temperature dependence of τ was observed for LCM *vs.* HCM. Least square fits to the inverse relaxation times (see ESI for details) indicate that Raman and direct processes dominate for HCM.[43] This

model was not sufficient to describe the relaxation in LCM, where an additional Orbach process[49] had to be included to reach satisfying agreement between simulation and experiment. Note, the Orbach relaxation process accelerates much faster with the temperature rise compared to power functions of direct and Raman processes. It results in steeper temperature dependence of τ for LCM group compared to HCM one. General increase in relaxation rate with increasing Co(II) concentration for both LCM and HCM groups is tentatively assigned to an increase of the intermolecular spin-spin interactions.

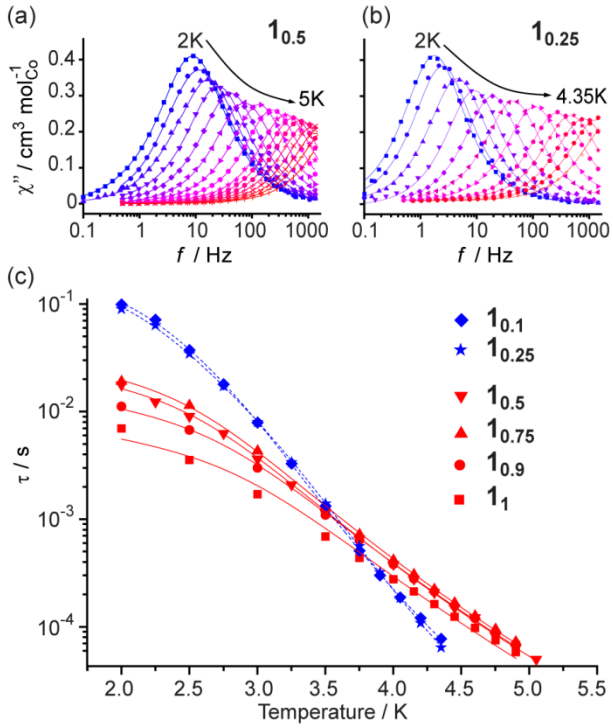

Figure 2: AC susceptibility data reveal difference in magnetic relaxation properties of HCM and LCM. (a) and (b) depict out-of-phase AC susceptibility traces, χ'', *vs.* frequency, *f*, for $\mathbf{1}_{0.5}$ and $\mathbf{1}_{0.25}$. (c) Extracted relaxation times τ show different temperature dependencies for LCM (blue symbols) and HCM (red symbols). Solid lines correspond to fits according to the Eq. S5 using best-fit parameters (Table S8).

Equilibrium magnetic properties are essential to understand dynamic magnetic properties, like relaxation of the magnetization. Furthermore, they are linked to the geometric and electronic structure via spin-orbit interaction. For the case of Co(II) (S = 3/2), the equilibrium magnetic properties are determined by the ground state Kramers doublet and the energy difference Δ to the first excited Kramers doublet (see Figure 3 and ESI). EPR is the method of choice to probe the transition energies between these levels. However, the relevant energies span several orders of magnitude, which urges for the application of EPR methods covering a very broad excitation energy range. We therefore combined very broadband THz-EPR and X-band EPR. THz-EPR allows for excitation of the inter doublet transitions and thereby a direct assignment of Δ, which is hardly possible with other methods.[23, 40, 50, 51] On the contrary, X-band EPR ($h\nu_{\mathrm{X-band}} \approx 0.33$ cm^{-1} $\ll \Delta$) detects transitions within the ground state doublet (see Figure 3 (b) and 2 (c)), which are most sensitive to the rhombicity and the type of anisotropy.[52]

THz-EPR revealed Δ = 75 cm^{-1} and Δ = 49 cm^{-1} for HCM and LCM, respectively (see Figure 3a and the ESI for further data). X-band EPR on HCM exhibits essentially all identical resonance fields of 115 mT, 170 mT, and 325 mT, while for LCM resonance fields at 100 mT, 745 mT, and 875 mT were observed (see Figure 3 (b) and 3 (c), dashed vertical lines). Although the spectral shapes vary widely for LCM, the observed resonance fields were similar (see Figure S24). The observed resonance fields directly indicate easy-plane anisotropy for HCM and easy-axis anisotropy for LCM. In both series, the line width increases with increasing Co(II) concentration, which is tentatively assigned to an increase of dipolar spin-spin interactions.

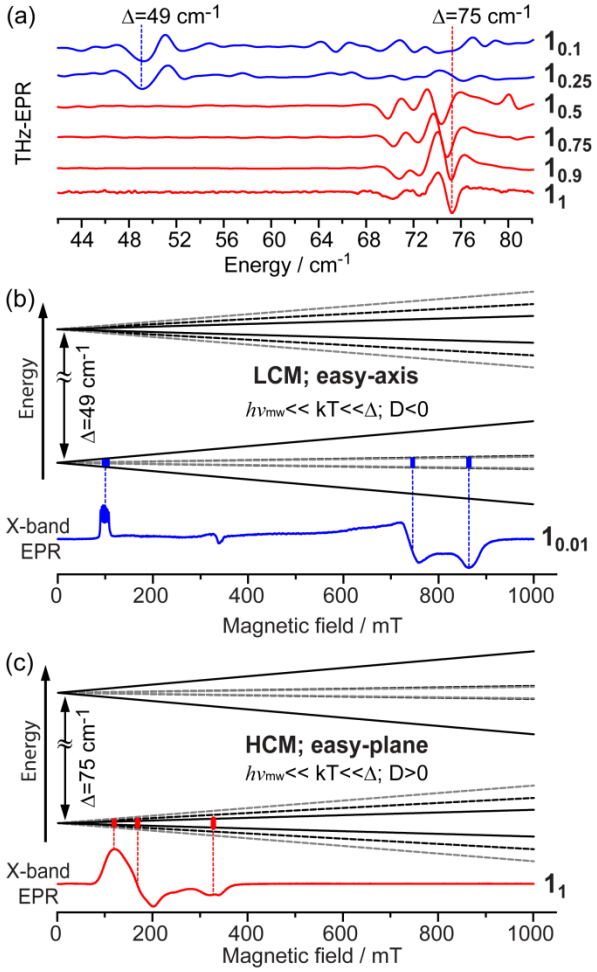

Figure 3: EPR allows assigning magnitude and sign of the magnetic anisotropy of LCM and HCM. (a) Depicts zero field THz-EPR spectra from which Δ = 75 cm^{-1} (HCM (red)) and Δ = 49 cm^{-1} (LCM (blue)) are determined. (b) Shows magnetic field dependent *S* = 3/2 energy levels for easy-axis (*D* < 0) anisotropy alongside a LCM X-band EPR spectrum (blue trace). Ground-state and excited-state doublets are plotted for magnetic fields parallel to the main anisotropy axis (solid black lines) and perpendicular to it (black and gray dashed lines). Resonance magnetic fields are assigned to the corresponding EPR transitions by blue dashed lines. (c) Shows orientation dependent spin energy levels and a HCM X-band EPR spectrum (red trace) for easy-plane (*D* > 0). Resonance fields are assigned to EPR transitions by red dashed lines.

For the simulation of EPR spectra shown in the SI and the calculation of the spin energy levels depicted in Figure 3 (b) and (c) an effective spin S = 3/2 Hamiltonian (SH) was employed:

$$\hat{H}_{3/2} = D\left(\hat{S}_z^2 - \frac{1}{3}\hat{\boldsymbol{S}}^2\right) + E\left(\hat{S}_x^2 - \hat{S}_y^2\right) + \mu_B \boldsymbol{B}_0 \cdot \boldsymbol{g} \cdot \hat{\boldsymbol{S}} \qquad (1)$$

The first and the second terms account for the zero-field splitting (ZFS), with the axial and rhombic ZFS parameters D and E, respectively. By definition, $0 \leq E/D \leq \frac{1}{3}$, and the *z*-axis is the unique anisotropy axis. For positive D, this is the hard axis, and for negative D the easy axis. The energy difference between the doublets is $\Delta = 2\sqrt{D^2 + 3E^2}$. The third term in equation 1 is the anisotropic Zeeman interaction, where the $\boldsymbol{g}$-tensor is assumed to be diagonal and axial, *i.e.* $\boldsymbol{g} = \mathrm{diag}(g_\perp, g_\perp, g_{||})$.

The following SH parameters were determined from spectral simulations:

HCM: D = 36.7 cm^{-1}, E = 4.5 cm^{-1}, $g_\perp$ = 2.53, $g_{||}$ = 2.21

LCM: D = -23.9 cm^{-1}, E = 3.1 cm^{-1}, $g_\perp$ = 2.25, $g_{||}$ = 2.38

The final missing link between the geometric and electronic structures on the one hand and the magnetic properties on the other hand is accessible through quantum chemical calculations.[22, 53] *Ab initio* calculations were performed for a single molecule with Co(II) in the experimentally obtained structures of **1$_1$**, **1$_{0.9}$**, **1$_{0.75}$**, **1$_{0.5}$**, **1$_{0.25}$**, **1$_{0.1}$** and (the fictitious) **1$_0$**. Calculated Δ were 82 cm^{-1}, 78 cm^{-1}, 77 cm^{-1}, 76 cm^{-1}, 45 cm^{-1}, 44 cm^{-1} and 43 cm^{-1}, respectively. These values match the experimental results very well. The trends in the calculated Δ can be directly assigned to the trends in the bond lengths (see Fig. 1c and ESI). In the following, **1$_1$** is discussed as representative for HCM and **1$_0$** for LCM. The calculated magnetic anisotropy tensors of the ground doublet state (see Fig. 1 (a), (b) and ESI) show a clear difference: it is oblate for **1$_1$** and prolate for **1$_0$**, hence they have easy-plane and easy-axis anisotropy, respectively. In a simplified model, contributions of orbital states to the calculated D values (Table S11) were analyzed.[12, 22] For **1$_1$**, the first and second excited states contribute significantly. They can be mixed with the ground state by the operators $\hat{L}_x$ and $\hat{L}_y$, but not by $\hat{L}_z$, therefore D is positive. In **1$_0$**, the first excited state has the main contribution to D, and this state can be mixed with the ground state only by $\hat{L}_z$, resulting in negative D.

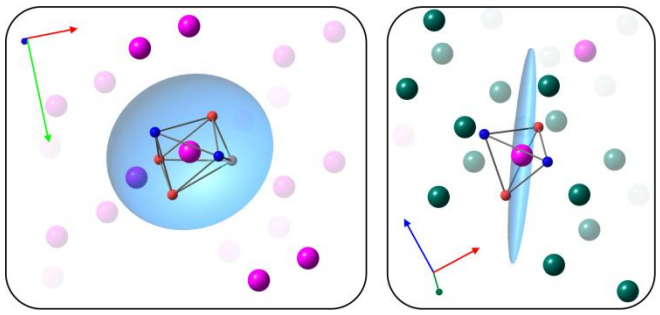

Figure 4: Schematic view of Co(II) surrounded by other Co(II) (left, HCM) and Zn(II) (right, LCM). In HCM, all or the majority of complexes contain Co(II), with a distorted octahedral ligand environment and easy-plane type of anisotropy, depicted by an oblate tensor. In the LCM counterparts, Co(II) containing complexes are a minority. The remaining Co(II) are in a distorted tetrahedral ligand environment, resulting in easy-axis magnetic anisotropy (prolate tensor). Differences in the crystal packing and the size of the unit cell are indicated by different box sizes.

Based on the assignment of the anisotropy, the magnetization dynamics may be rationalized. Clearly different magnetic properties between HCM and LCM were measured, while inside each group the magnetic properties were found, basically, identical. HCM showed significant easy-plane anisotropy. For this type of anisotropy, the energy barrier for reorientation of the magnetization from one ground state to the other vanishes. Indeed, we could fit the (inverse) relaxation times obtained by AC susceptibility without account of any barriers and related processes, and this additionally supports the easy-plane anisotropy. In turn, LCM showed significant easy-axis anisotropy and an Orbach process, *i.e.* thermal relaxation over an energy barrier, had to be included additionally to describe the AC susceptibility results.

3. Conclusions and Outlook

[Co(piv)$_2$(2-NH$_2$-Py)$_2$] is a high-spin (S = 3/2) complex with an easy-plane magnetic anisotropy characterized by an energy difference Δ between the Kramers doublets of ~75 cm^{-1}. Diamagnetic dilution of this complex by Zn^{II} ([Co$_x$Zn$_{1-x}$(piv)$_2$(2-NH$_2$-Py)$_2$]) has a minor impact on its structural and magnetic properties as long as x=1÷0.5. In this range of x both molecules [Co(piv)$_2$(2-NH$_2$-Py)$_2$] and [Zn(piv)$_2$(2-NH$_2$-Py)$_2$] adopt the same distorted octahedral coordination geometry corresponding to that of pure Co^{II} complex. In contrast, further decrease of Co^{II} concentration down to x = 0.25 switches the whole structure to that of pure [Zn(piv)$_2$(2-NH$_2$-Py)$_2$]. At x ≤0.25 the molecules of [Co(piv)$_2$(2-NH$_2$-Py)$_2$] adopt the structure of the host diamagnetic lattice (distorted tetrahedral coordination geometry), leading to dramatic changes in the observed magnetic properties. Indeed, apart from an abrupt change of the magnitude of Δ from ~75 cm^{-1} to ~49 cm^{-1}, the ZFS parameters D changes its sign from positive to negative, meaning that the magnetic anisotropy changes its type from easy-plane to easy-axis. This results in a slow-down of magnetic relaxation at low temperatures.

The observed inversion of magnetic anisotropy upon isolation of the SIM in the diamagnetic lattice results in a fundamental improvement of the SIM properties of this compound. This may be regarded as a lucky, occasional finding and specific to the observed system. However, the importance of the outlined study reaches far beyond the reported single case. Findings shown here can be extended and transformed into a new strategy in design of magnetic memory units or other spin devices based on the isolated SIMs. In this strategy, structural and magnetic properties of the bulk magnetically-concentrated SIM are of the secondary importance. Instead, a suitable diamagnetic host compound should be searched for, whose structure of coordination sites would potentially enable the desired SIM properties upon doping of magnetoactive metals. Even complexes, which have been initially sorted out due to their "wrong" magnetic properties, may be reconsidered based on the knowledge-driven approach described herein.

Our present work underlines the great potential of *ab initio* calculations in preliminary estimation of magnetic properties of such engineered SIMs. Large number of database-listed structurally characterized SIM candidates and their diamagnetic analogs can be examined by means of quantum chemical calculations for desired properties of magnetically diluted SIMs. Next, SQUID, EPR and FD-FT THz-EPR are the indispensable techniques to validate SIM

properties experimentally, where the EPR-based methods have high sensitivity to study magnetic properties of even strongly diluted systems.

Finally, we anticipate that a similar improvement of magnetic anisotropy upon isolation in a diamagnetic lattice should occur not only in Co^{II}-based SIMs, but also in other types of SIMs and SMMs, because there is a simple structural reason behind it. Therefore, the proposed strategy might become broadly used in the future for designing the building blocks of diverse spintronics devices.

4. Experimental

4.1 Synthesis. Crystalline materials of the complexes $[Co_xZn_{(1-x)}(piv)_2(2\text{-}NH_2\text{-}Py)_2]$ (**1*x***, with *x* = 1, 0.9, 0.75, 0.5, 0.25, 0.1, 0.03, 0.01, 0) were obtained according to procedures described elsewhere for **1**$_1$,[54] and in the ESI. Powder X-Ray Diffraction (PXRD) was performed on a Bruker D8 Advance diffractometer (CuK_α, λ = 1.54 Å, Ni-filter, LYNXEYE detector, geometry reflection) at room temperature. Infrared (IR) spectra in the range 400–4000 cm^{-1} were measured on a Fourier-Transform IR (FT-IR) Perkin Elmer Spectrum-65LS spectrometer with Specac's high performance single reflection monolithic diamond attenuated total reflection (ATR) accessory. Elemental analysis was carried out on an EA1108 Carlo Erba automatic CHNS-analyzer. Energy-dispersive X-ray (EDX) analysis was performed in the mapping mode on an Oxford Instruments X-MAX EDX analyzer for the determination of Co:Zn ratios.

Diffraction data for all complexes was collected on a Bruker SMART APEX II diffractometer equipped with a charge-coupled device (CCD) detector (graphite monochromator, λ(MoKα) = 0.71073 Å).[55] Absorption correction was applied based on the intensities of equivalent reflections with the SADABS program.[56] The structures of all compounds were solved by the direct method and refined by the full-matrix least squares technique in the anisotropic approximation (except hydrogen atoms) using the SHELX-2014 software. The positions of the hydrogen atoms in the organic ligands were calculated geometrically and refined in the riding model (in some structures H atoms in NH_2-groups could be located by Fourier maps).

4.2 Magnetometry. AC magnetic susceptibility data was collected on a Quantum Design MPMS-XL SQUID magnetometer on finely ground polycrystalline powders (~20 mg) in the temperature range of 2-5 K under a DC field of 0.2 T and an AC field of 0.35 mT oscillating in a frequency range of 0.1-1500 Hz.

4.3 THz-EPR. Frequency Domain Fourier Transform THz EPR (THz-EPR) at external magnetic fields from 0 to 10 T was performed at the THz beamline of the synchrotron radiation facility BESSY II in Voigt configuration and with a Hg arc lamp as THz source.[50, 57, 58] THz-EPR samples were prepared as pellets containing typically 20 mg of **1*x*** mixed with approximately 100 mg of polyethylene powder. Experiments were performed at low temperatures. If not stated otherwise, the temperature was 5 K. Experimental resolution was 0.2 cm^{-1} (experiments on **1**$_1$ and **1**$_{0.1}$) or 1 cm^{-1} (all other samples). A 6 µm Mylar Multilayer beam splitter was used and the signals were detected with a 4.2 K Si bolometer (Infrared Laboratories). THz-EPR spectra are shown as magnetic field division spectra (MDS), obtained by dividing spectra measured at an external magnetic field B_0 by a reference spectrum measured at B_0+ 1 T.[50]

3.4 X-Band EPR. Continuous wave (CW) X-band (9.7 GHz) EPR measurements were carried out on a Bruker Elexsys E580 spectrometer, equipped with an Oxford Instruments He cryostat (ER 4118CF-O) and temperature controller ITC 503S. A Bruker ER 4118X-MD5 resonator was modified by replacing the dielectric sapphire insert by bismuth germanate (3 mm inner diameter) to suppress the resonator background.[59] X-band EPR spectra were recorded at a microwave power of ~1.9 mW and a Lock-In modulation amplitude of 0.5 mT. X-band EPR samples of **1*x*** with Co(II) amounts *x* = 1÷0.1 were ground and mixed with quartz powder. For each sample the quantity of quartz was approximately 20 mg, the amount of **1*x*** increased from ~2 mg to ~10 mg upon decreasing *x*. Samples with *x* = 0.03 and 0.01 were ground and used without additions. The weighted quantity of ground samples (~15 mg, polycrystalline powder) was placed in a 2.8 mm outer diameter EPR tube, evacuated (10^{-2} mbar) and fused. Both, THz-EPR and X-band EPR data was simulated with the *EasySpin* toolbox.[60-62]

4.5 Quantum Chemical Calculations. State-averaged complete active space self-consisted field (SA-CASSCF) [63-65] calculations were performed using experimentally obtained structures (always assuming a Co atom at the metal position, irrespective of the value of x) without further geometry optimizations. The segmented all-electron relativistically contracted version[66] of Ahlrichs polarized basis set def2-TZVP was used.[67-69] To speed up calculations, the resolution of identity approximation with corresponding correlation fitting of the basis set was employed.[70] Dynamic correlations and scalar relativistic effects were taken into account by N-electron valence perturbation theory to second order (NEVPT2),[71, 72] and by the second-order Douglas-Kroll-Hess (DKH) procedure,[73, 74] respectively. The complete active space CAS (7, 5) contained seven electrons in five d-orbitals. All 10 quartet and 40 doublet states of Co(II) were included. The fine structure of ground and excited states were computed within the Breit-Pauli approximation and the mean field approximation (SOMF).[75] Spin Hamiltonian (SH) parameters and g-factors have been computed by second order perturbation theory (PT2)[76] and with an effective Hamiltonian (QDPT).[75, 77] All quantum chemical calculations were performed with the ORCA computational program package.[78]

Author contributions

S.L.V. and J.N. conceived the research. M.A.K. synthesized the molecules, performed chemical characterizations and X-ray analyses. I.A.V., A.S.B., V.I.O., S.L.V. performed and analyzed AC susceptibility experiments. I.A.V., A.M.S., M.V.F. and S.L.V. performed and analyzed the X-Band EPR experiments. J.N., I.A.V., K.H., and S.L.V. performed the THz-EPR experiments with support of A.S. J.N., with support of C. H., and E.A.S. performed and analyzed ab initio calculations. J.N., A.S, M.V.F, E.A.S, and S.L.V. wrote the manuscript with contributions from all authors. A.S. and S.V. oversaw the project.

Conflicts of interest

There are no conflicts to declare.

Acknowledgements

Financial support by the Russian Science Foundation through grant no. 17-13-01412 (X-band EPR measurements) and by the Deutsche Forschungsgemeinschaft (DFG) through priority program SPP 1601 and a Research Fellowship to J.N. (grant no. NE 2064/1-1 FOR) is thankfully acknowledged. J.N., I.A.V., and S.L.V. thankfully

acknowledge the financial support from HZB. J.N. and A.S. acknowledge funding through the Max Planck Society. M.A.K. is grateful for financial support from the State Assignment on Fundamental Research of the Kurnakov Institute of General and Inorganic Chemistry of RAS (IGIC RAS) and thank the User Facilities Centers of IGIC RAS for the facility to do X-ray, IR and elemental analysis measurements. V.I.O. and A.S.B. acknowledge Russian Science Foundation (project 18-13-00380) for support of the SQUID measurements. E.A.S acknowledges Russian Science Foundation (project 16-13-10155) and Supercomputer center of the Novosibirsk State University for support of the computational part of this work. J.N. and C.H. thank the University of Hamburg High Performance Computing Centre (RRZ) for computational resources. We thank Dirk Ponwitz (HZB) for technical support, Dr. Ekaterina Zorina-Tikhonova (IGIC RAS) for IR data interpretation and Dr. Alexander Baranchikov (IGIC RAS) for EDX analysis.

References

1. L. Bogani and W. Wernsdorfer, *Nat. Mater.*, 2008, **7**, 179-186.
2. A. Cornia, A. F. Costantino, L. Zobbi, A. Caneschi, D. Gatteschi, M. Mannini and R. Sessoli, in *Single-Molecule Magnets and Related Phenomena*, ed. R. Winpenny, Springer Berlin Heidelberg, Berlin, Heidelberg, 2006, DOI: 10.1007/430_029, pp. 133-161.
3. M. N. Leuenberger and D. Loss, *Nature*, 2001, **410**, 789-793.
4. M. Mannini, F. Pineider, P. Sainctavit, C. Danieli, E. Otero, C. Sciancalepore, A. M. Talarico, M.-A. Arrio, A. Cornia, D. Gatteschi and R. Sessoli, *Nat. Mater.*, 2009, **8**, 194-197.
5. G. Aromí, D. Aguilà, P. Gamez, F. Luis and O. Roubeau, *Chem. Soc. Rev.*, 2012, **41**, 537-546.
6. A. Gaita-Ariño, F. Luis, S. Hill and E. Coronado, *Nature Chemistry*, 2019, **11**, 301-309.
7. D. Gatteschi, R. Sessoli and J. Villain, *Molecular Nanomagnets*, OUP Oxford, 2006.
8. F. Neese and D. A. Pantazis, *Faraday Discussions*, 2011, **148**, 229-238.
9. M. Atanasov, J. M. Zadrozny, J. R. Long and F. Neese, *Chem. Sci.*, 2013, **4**, 139-156.
10. C. J. Milios, R. Inglis, A. Vinslava, R. Bagai, W. Wernsdorfer, S. Parsons, S. P. Perlepes, G. Christou and E. K. Brechin, *Journal of the American Chemical Society*, 2007, **129**, 12505-12511.
11. J. D. Rinehart and J. R. Long, *Chem. Sci.*, 2011, **2**, 2078-2085.
12. S. Gómez-Coca, D. Aravena, R. Morales and E. Ruiz, *Coordination Chemistry Reviews*, 2015, **289-290**, 379-392.
13. F.-S. Guo, B. M. Day, Y.-C. Chen, M.-L. Tong, A. Mansikkamäki and R. A. Layfield, *Science*, 2018, **362**, 1400-1403.
14. K. Randall McClain, C. A. Gould, K. Chakarawet, S. J. Teat, T. J. Groshens, J. R. Long and B. G. Harvey, *Chem. Sci.*, 2018, **9**, 8492-8503.
15. C. A. P. Goodwin, F. Ortu, D. Reta, N. F. Chilton and D. P. Mills, *Nature*, 2017, **548**, 439-442.
16. F. S. Guo, B. M. Day, Y. C. Chen, M. L. Tong, A. Mansikkamaki and R. A. Layfield, *Science*, 2018, **362**, 1400-+.
17. J. M. Frost, K. L. M. Harriman and M. Murugesu, *Chem. Sci.*, 2016, **7**, 2470-2491.
18. S. Gomez-Coca, D. Aravena, R. Morales and E. Ruiz, *Coordination Chemistry Reviews*, 2015, **289**, 379-392.
19. M. Murrie, *Chem. Soc. Rev.*, 2010, **39**, 1986-1995.
20. Y.-Y. Zhu, C. Cui, Y.-Q. Zhang, J.-H. Jia, X. Guo, C. Gao, K. Qian, S.-D. Jiang, B.-W. Wang, Z.-M. Wang and S. Gao, *Chem. Sci.*, 2013, **4**, 1802-1806.
21. P. C. Bunting, M. Atanasov, E. Damgaard-Moller, M. Perfetti, I. Crassee, M. Orlita, J. Overgaard, J. van Slageren, F. Neese and J. R. Long, *Science*, 2018, **362**, 1378-+.
22. E. A. Suturina, D. Maganas, E. Bill, M. Atanasov and F. Neese, *Inorganic Chemistry*, 2015, **54**, 9948-9961.
23. Y. Rechkemmer, F. D. Breitgoff, M. van der Meer, M. Atanasov, M. Hakl, M. Orlita, P. Neugebauer, F. Neese, B. Sarkar and J. van Slageren, *Nat. Commun.*, 2016, **7**.
24. V. V. Novikov, A. A. Pavlov, Y. V. Nelyubina, M. E. Boulon, O. A. Varzatski, Y. Z. Voloshin and R. E. P. Winpenny, *Journal of the American Chemical Society*, 2015, **137**, 9792-9795.
25. X. N. Yao, J. Z. Du, Y. Q. Zhang, X. B. Leng, M. W. Yang, S. D. Jiang, Z. X. Wang, Z. W. Ouyang, L. Deng, B. W. Wang and S. Gao, *Journal of the American Chemical Society*, 2017, **139**, 373-380.
26. M. Shiddiq, D. Komijani, Y. Duan, A. Gaita-Ariño, E. Coronado and S. Hill, *Nature*, 2016, **531**, 348-351.
27. D. Gatteschi, A. Cornia, M. Mannini and R. Sessoli, *Inorganic Chemistry*, 2009, **48**, 3408-3419.
28. F. Allouche, G. Lapadula, G. Siddiqi, W. W. Lukens, O. Maury, B. Le Guennic, F. Pointillart, J. Dreiser, V. Mougel, O. Cador and C. Coperet, *ACS Central Sci.*, 2017, **3**, 244-249.
29. C. H. Chen, D. S. Krylov, S. M. Avdoshenko, F. Liu, L. Spree, R. Westerstrom, C. Bulbucan, M. Studniarek, J. Dreiser, A. U. B. Wolter, B. Buchner and A. A. Popov, *Nanoscale*, 2018, **10**, 11287-11292.
30. A. Cornia, M. Mannini, P. Sainctavit and R. Sessoli, *Chem. Soc. Rev.*, 2011, **40**, 3076-3091.
31. J. Liu, Y. C. Chen, J. L. Liu, V. Vieru, L. Ungur, J. H. Jia, L. F. Chibotaru, Y. H. Lan, W. Wernsdorfer, S. Gao, X. M. Chen and M. L. Tong, *J Am Chem Soc*, 2016, **138**, 5441-5450.
32. F. Habib, P. H. Lin, J. Long, I. Korobkov, W. Wernsdorfer and M. Murugesu, *J Am Chem Soc*, 2011, **133**, 8830-8833.
33. F. Habib, I. Korobkov and M. Murugesu, *Dalton T*, 2015, **44**, 6368-6373.
34. J. M. Zadrozny and J. R. Long, *J Am Chem Soc*, 2011, **133**, 20732-20734.
35. W. Huang, T. Liu, D. Y. Wu, J. J. Cheng, Z. W. Ouyang and C. Y. Duan, *Dalton T*, 2013, **42**, 15326-15331.
36. Z. B. Hu, X. Feng, J. Li, Y. Q. Zhang, L. Yin, Z. X. Wang, Z. W. Ouyang, M. Kurmoo and Y. Song, *Dalton Transactions*, 2020, **49**, 2159-2167.

37. M. Ceglarska, O. Stefanczyk, S. I. Ohkoshi and A. M. Majcher-Fitas, *Dalton Transactions*, 2020, **49**, 6807-6815.
38. K. R. Meihaus, J. D. Rinehart and J. R. Long, *Inorg Chem*, 2011, **50**, 8484-8489.
39. S. Titos-Padilla, J. Ruiz, J. M. Herrera, E. K. Brechin, W. Wersndorfer, F. Lloret and E. Colacio, *Inorg Chem*, 2013, **52**, 9620-9626.
40. M. A. Palacios, J. Nehrkorn, E. A. Suturina, E. Ruiz, S. Gomez-Coca, K. Holldack, A. Schnegg, J. Krzystek, J. M. Moreno and E. Colacio, *Chem.-Eur. J.*, 2017, **23**, 11649-11661.
41. J. Li, Y. Han, F. Cao, R. M. Wei, Y. Q. Zhang and Y. Song, *Dalton T*, 2016, **45**, 9279-9284.
42. R. Ruamps, L. J. Batchelor, R. Guillot, G. Zakhia, A. L. Barra, W. Wernsdorfer, N. Guihery and T. Mallah, *Chem Sci*, 2014, **5**, 3418-3424.
43. S. Gomez-Coca, A. Urtizberea, E. Cremades, P. J. Alonso, A. Camon, E. Ruiz and F. Luis, *Nat. Commun.*, 2014, **5**.
44. R. Docherty, F. Tuna, C. A. Kilner, E. J. L. McInnes and M. A. Halcrow, *Chem. Commun.*, 2012, **48**, 4055-4057.
45. H. Daubric, R. Berger, J. Kliava, G. Chastanet, O. Nguyen and J. F. Letard, *Phys. Rev. B*, 2002, **66**.
46. S. V. Tumanov, S. L. Veber, S. Greatorex, M. A. Halcrow and M. V. Fedin, *Inorganic Chemistry*, 2018, **57**, 8709-8713.
47. S. Alvarez, D. Avnir, M. Llunell and M. Pinsky, *New J. Chem.*, 2002, **26**, 996-1009.
48. D. Gatteschi, R. Sessoli and J. Villain, *MOLECULAR NANOMAGNETS INTRODUCTION*, Oxford Univ Press, New York, 2006.
49. A. Abragam and B. Bleaney, *Electron Paramagnetic Resonance of Transition Ions*, Oxford University Press, 1970.
50. J. Nehrkorn, K. Holldack, R. Bittl and A. Schnegg, *J. Magn. Reson.*, 2017, **280**, 10-19.
51. E. A. Suturina, J. Nehrkorn, J. M. Zadrozny, J. Liu, M. Atanasov, T. Weyhermuller, D. Maganas, S. Hill, A. Schnegg, E. Bill, J. R. Long and F. Neese, *Inorganic Chemistry*, 2017, **56**, 3102-3118.
52. J. R. Pilbrow, *Transition Ion Electron Paramagnetic Resonance*, Clarendon Press, 1990.
53. M. Atanasov, D. Aravena, E. Suturina, E. Bill, D. Maganas and F. Neese, *Coordination Chemistry Reviews*, 2015, **289**, 177-214.
54. N. A. Bokach, V. Y. Kukushkin, M. Haukka, T. B. Mikhailova, A. A. Sidorov and I. L. Eremenko, *Russ. Chem. Bull.*, 2006, **55**, 36-43.
55. *Journal*.
56. *Journal*.
57. J. Nehrkorn, B. M. Martins, K. Holldack, S. Stoll, H. Dobbek, R. Bittl and A. Schnegg, *Mol. Phys.*, 2013, **111**, 2696-2707.
58. A. Schnegg, J. Behrends, K. Lips, R. Bittl and K. Holldack, *Physical Chemistry Chemical Physics*, 2009, **11**, 6820-6825.
59. M. Y. Ivanov, V. A. Nadolinny, E. G. Bagryanskaya, Y. A. Grishin, M. V. Fedin and S. L. Veber, *J. Magn. Reson.*, 2016, **271**, 83-89.
60. J. Nehrkorn, J. Telser, K. Holldack, S. Stoll and A. Schnegg, *J. Phys. Chem. B*, 2015, **119**, 13816-13824.
61. J. Nehrkorn, A. Schnegg, K. Holldack and S. Stoll, *Phys. Rev. Lett.*, 2015, **114**.
62. S. Stoll and A. Schweiger, *J. Magn. Reson.*, 2006, **178**, 42-55.
63. B. O. Roos, P. R. Taylor and P. E. M. Siegbahn, *Chem. Phys.*, 1980, **48**, 157-173.
64. P. Siegbahn, A. Heiberg, B. Roos and B. Levy, *Phys. Scr.*, 1980, **21**, 323-327.
65. P. E. M. Siegbahn, J. Almlof, A. Heiberg and B. O. Roos, *J. Chem. Phys.*, 1981, **74**, 2384-2396.
66. D. A. Pantazis, X. Y. Chen, C. R. Landis and F. Neese, *J. Chem. Theory Comput.*, 2008, **4**, 908-919.
67. A. Schafer, H. Horn and R. Ahlrichs, *J. Chem. Phys.*, 1992, **97**, 2571-2577.
68. F. Weigend and R. Ahlrichs, *Physical Chemistry Chemical Physics*, 2005, **7**, 3297-3305.
69. A. Schafer, C. Huber and R. Ahlrichs, *J. Chem. Phys.*, 1994, **100**, 5829-5835.
70. F. Neese, *J. Comput. Chem.*, 2003, **24**, 1740-1747.
71. C. Angeli, R. Cimiraglia and J. P. Malrieu, *J. Chem. Phys.*, 2002, **117**, 9138-9153.
72. C. Angeli, R. Cimiraglia and J. P. Malrieu, *Chem. Phys. Lett.*, 2001, **350**, 297-305.
73. B. A. Hess, *Phys. Rev. A*, 1986, **33**, 3742-3748.
74. M. Douglas and N. M. Kroll, *Annals of Physics*, 1974, **82**, 89-155.
75. D. Ganyushin and F. Neese, *J. Chem. Phys.*, 2013, **138**.
76. F. Neese and E. I. Solomon, *Inorganic Chemistry*, 1998, **37**, 6568-6582.
77. R. Maurice, R. Bastardis, C. de Graaf, N. Suaud, T. Mallah and N. Guihery, *J. Chem. Theory Comput.*, 2009, **5**, 2977-2984.
78. F. Neese, *Wiley Interdiscip. Rev.-Comput. Mol. Sci.*, 2012, **2**, 73-78.